






## Terahertz displacive excitation of a coherent Raman-active phonon in $V_2O_3$

Flavio Giorgianni <sup>1✉</sup>, Mattia Udina<sup>2</sup>, Tommaso Cea<sup>3</sup>, Eugenio Paris <sup>4</sup>, Marco Caputo<sup>5</sup>, Milan Radovic <sup>5</sup>, Larissa Boie <sup>6</sup>, Joe Sakai<sup>7</sup>, Christof W. Schneider<sup>8</sup> & Steven Lee Johnson <sup>4,6</sup>

Nonlinear processes involving frequency-mixing of light fields set the basis for ultrafast coherent spectroscopy of collective modes in solids. In certain semimetals and semiconductors, generation of coherent phonon modes can occur by a displacive force on the lattice at the difference-frequency mixing of a laser pulse excitation on the electronic system. Here, as a low-frequency counterpart of this process, we demonstrate that coherent phonon excitations can be induced by the sum-frequency components of an intense terahertz light field, coupled to intraband electronic transitions. This nonlinear process leads to charge-coupled coherent dynamics of Raman-active phonon modes in the strongly correlated metal  $V_2O_3$ . Our results show an alternative up-conversion pathway for the optical control of Raman-active modes in solids mediated by terahertz-driven electronic excitation.

<sup>1</sup>Paul Scherrer Institute, 5232 Villigen-PSI, Switzerland. <sup>2</sup>ISC-CNR and Department of Physics, “Sapienza” University of Rome, P.le Aldo Moro 5, 00185 Rome, Italy. <sup>3</sup>IMDEA Nanoscience, C/Farady 9, 28049 Madrid, Spain. <sup>4</sup>SwissFEL, Paul Scherrer Institute, 5232 Villigen-PSI, Switzerland. <sup>5</sup>Photon Science Division, Paul Scherrer Institute, 5232 Villigen-PSI, Switzerland. <sup>6</sup>Institute for Quantum Electronics, Physics Department, ETH Zurich, Auguste-Piccard-Hof 1, 8093 Zurich, Switzerland. <sup>7</sup>Institut Català de Nanociència i Nanotecnologia (ICN2), UAB Campus, ICN2 Building, 08193 Bellaterra, Spain. <sup>8</sup>Laboratory for Multiscale Materials Experiments, Paul Scherrer Institut, CH-5232 Villigen PSI, Switzerland. ✉email: [flavio.giorgianni@psi.ch](mailto:flavio.giorgianni@psi.ch)

Phononics has recently been proposed as a promising avenue towards a new generation of faster and more efficient technologies<sup>1</sup>. Phenomena associated with lattice dynamics are often analogous to well-known effects involving electrons, for example chirality and the phonon Hall effect<sup>2–4</sup>. Moreover, control over coherent phonons offers potential new pathways to drive transitions between phases in condensed matter and to coherently manipulate the ground state of magnetically ordered phases<sup>5–11</sup>. While coherent acoustic phonon modes are commonly generated by wide variety of mechanisms<sup>12</sup>, higher-frequency coherent optical phonon modes are typically driven from interactions with intense sub-picosecond light pulses<sup>13</sup>.

In most cases, light pulses can drive optical phonons either directly *via* resonant electric-dipole interaction<sup>14,15</sup>, or indirectly *via* interactions with electronic states or other phonon modes<sup>10,16–18</sup>. The latter case is a generalization of the stimulated Raman mechanism, in which the ultrashort light pulse couples to the electronic system resulting in a nonlinear force on the lattice that resonantly drives coherent phonon modes at the difference frequency mixing  $\Omega = \omega_1 - \omega_2$ , with  $\omega_1$  and  $\omega_2$  taken for the pulse spectrum. This is commonly referred to in the literature as either Impulsive Stimulated Raman Scattering (ISRS), when the light field is non-resonantly coupled to the electric system (in optically transparent solids), or Displacive Excitation of Coherent Phonons (DECP), when the light pulse is resonant with intraband or interband electronic transitions (in opaque solids)<sup>19–23</sup>. Unlike ISRS, which involves non-resonant coupling to electronic states to produce impulsive excitation, in the DECP regime, coherent phonons are generated by a displacive force associated with a sudden change in carrier density or electronic temperature induced by the intense light pulse. A third generation mechanism is called Ionic Raman scattering (IRS) and involves a higher frequency phonon mode that serves as the intermediate<sup>18</sup>. In all these processes, the driving mechanism involves difference-frequency mixing, and requires the bandwidth of the driving light pulse to be comparable to or larger than the frequency of the optical phonon mode that is to be excited<sup>24</sup>.

As an alternative to these well-established routes for coherent phonon generation using stimulated Raman schemes, it is also possible to drive coherent Raman-active vibrational modes using sum-frequency excitation (SFE)<sup>25,26</sup>. Recent experiments, indeed, have demonstrated both photonic and phononic SFE mechanisms<sup>25,27–30</sup>, which involve the absorption of two photons or two phonons with frequencies  $\omega_1$  and  $\omega_2$  to create one phonon in a Raman-active mode at frequency  $\Omega = \omega_1 + \omega_2$ , as up-conversion counterparts of ISRS and IRS, respectively.

Here, we demonstrate an alternative scheme for coherent generation of Raman-active phonon modes based on terahertz-driven displacive excitation as up-conversion counterpart of the DECP mechanism. An intense THz pulse, inducing strong transient electronic excitation, is found to generate large-amplitude coherent oscillations of Raman-active phonon modes in the metallic phase of  $V_2O_3$  at twice the frequency of the driving field. This nonlinear process can be described as a displacive excitation that involves the sum-frequency mixing component of the THz pulse coupled to the electronic system. The temperature dependence of the generated coherent phonons supports the scenario in which the excitation process is strongly enhanced by intra-band electronic transitions driven by the intense THz field.

## Results

**Coherent phonon oscillations detected by THz pump – near-infrared probe spectroscopy.** In  $V_2O_3$ , strong electronic correlations cause a metal-insulator transition (MIT) at  $T_{MIT} \approx 150$  K, which is accompanied by a first-order structural transition from

corundum to monoclinic<sup>31,32</sup>. Recent experiments have shown that the coherent lattice displacement generated by perturbing the electronic distribution of strongly correlated metallic phase of  $V_2O_3$  through ultrafast light excitation can drive both longitudinal acoustic waves and optical phonons<sup>33–37</sup>. In these photoexcitation processes, the electron-phonon coupling plays a central role in the transient atomic displacement of the structure<sup>38</sup>.

Figure 1a shows the schematic electronic energy levels for the metallic phase of  $V_2O_3$ . The Fermi energy crosses the partially filled  $a_{1g}$  and  $e_g^*$  bands, enabling the direct optical absorption of THz light by intraband electronic transitions<sup>31,32</sup>. The  $\Gamma$ -point structural dynamics in this phase is largely dominated by a fully-symmetric  $A_{1g}$  optical phonon mode at  $\Omega/2\pi = 7.1$  THz, which corresponds to the optical bending mode of the  $V_2O_2$  unit cell [see displacement vectors in Fig. 1b<sup>35,39</sup>]. Other Raman-active optical phonons in this frequency range, for example the  $E_g$  phonon mode at  $\sim 6$  THz<sup>39</sup>, have a comparatively lower Raman cross-section, as detailed in the Supplementary Note 3 and Supplementary Fig. 4.

To study the possibilities for driving coherent structural dynamics in  $V_2O_3$ , we performed ultrafast THz pump-optical probe spectroscopy (scheme shown in Fig. 1c). Intense quasi single-cycle THz pulses were focused onto the sample. The THz-induced response was monitored by measuring the optical transmission modulation  $\Delta T/T$  of a near-infrared (NIR) laser probe at 1.55 eV as a function of the time delay  $t_{pp}$  with respect to the pump<sup>25,40</sup>. The  $\Delta T/T$  response is able to detect the coherent lattice oscillations from the fully-symmetric  $A_{1g}$  *via* time-dependent modulation of the diagonal elements of the linear optical susceptibility tensor, while it is insensitive to the  $E_g$  modes, which effect the probe polarization state through the modulation of the off-diagonal elements of the susceptibility tensor (see detailed discussion in Supplementary Note 4).

The temporal waveform of the THz pump electric field  $E(t)$  (see Fig. 1d) was measured at the same position using electro-optic sampling from a GaP crystal (see Supplementary Methods). The center frequency of the pump is  $\nu_p \approx 3.5$  THz. The sample is a high-quality, 84 nm thick  $V_2O_3$  thin film epitaxially grown on an R-plane (1 -1 0 2) –  $Al_2O_3$  substrate (see Methods). Figure 1e shows the temporal evolution of the THz-induced transmission modulation  $\Delta T/T$ . The time origin ( $t_{pp} = 0$ ) is set to the delay where the optical probe interacts with the sample at the same time as does the peak of the square of the pump electric field  $|E(t)|^2$ . The observed THz-induced dynamics are dominated by coherent oscillations superimposed to a gradually increasing slowly-varying background. This long-lived step-like evolution of  $\Delta T/T$  is attributed to incoherent dynamics of the electronic thermalization through electron-phonon scattering, as described in refs. 33,35. Strikingly, the oscillating component of  $\Delta T/T$  clearly displays oscillations with a period shorter than the one of the THz driving field. To better show this feature, in Fig. 1f we compare the oscillatory component, obtained by subtracting the step-like background from  $\Delta T/T$ , with the intensity profile of the THz field  $|E(t)|^2$ . The fitting procedure for the background subtraction is reported in the Supplementary Note 4 and consists of Gaussian function to describe the THz excitation and a step-like function for the electronic relaxation dynamics as observed in refs. 33,35. To demonstrate that coherent oscillations originate from the  $V_2O_3$  thin film, we conducted the same experiment on the bare R-plane  $Al_2O_3$  substrate showing that there are neither oscillations nor a long-lived signal in the  $\Delta T/T$  dynamics, see Fig. 1f and Supplementary Note 2 for details. Furthermore, from Fig. 1f we note that the envelope function of the oscillatory response does not merely follow that of  $|E(t)|^2$ , but instead persists well beyond the times when the THz pulse intensity is negligible. This strongly suggests that the oscillations are indeed due to a coherent excitation of the  $A_{1g}$  mode in  $V_2O_3$  at its resonance frequency<sup>39</sup>.

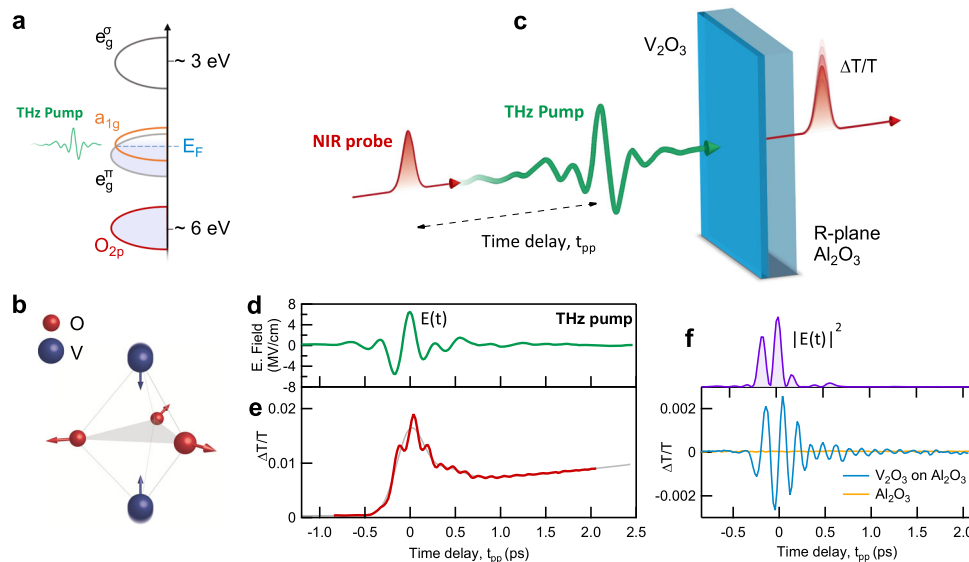


**Fig. 1** Coherent phonon generation by terahertz electronic excitations in  $V_2O_3$ . **a** Energy level diagram for the paramagnetic metallic phase of  $V_2O_3$  showing vanadium and oxygen energy levels. The Fermi energy  $E_F$  crosses the partially filled  $a_{1g}$  and  $e_g^\pi$  bands formed by vanadium 3d orbitals.  $O_{2p}$  bands lie between 3.5 and 8.5 eV below  $E_F$  while  $e_g^\sigma$  is centered at  $\sim 3$  eV above  $E_F$ . Level diagrams adapted from ref. 32. **b** Phonon displacement vectors of the  $A_{1g}$  phonon mode in  $V_2O_3$ . **c** Schematic of the setup for the THz pump-NIR probe experiment on  $V_2O_3$  thin film on R-plane  $Al_2O_3$  substrate to investigate the THz driven coherent lattice dynamics: intense THz pulse (green) excites the  $A_{1g}$  phonon mode, whose coherent dynamics are probed by a temporally delayed ultrashort optical pulse (red). **d** Waveform of THz pump electric field. The peak electric field is 6.5 MV/cm. **e** Probe transmission modulation signal  $\Delta T/T$  as a function of the pump-probe delay  $t_{pp}$ . The THz pump pulse induces coherent lattice oscillations related to the fully-symmetric  $A_{1g}$  phonon at approximately twice the frequency of the driving electric field. The red curve represents the experimental data. Gray curve represents the slowly-varying background as determined by double-exponential relaxation fitting procedure (see Supplementary Note 4). **f** Light-blue curve shows the oscillatory component of  $\Delta T/T$  time-trace of  $V_2O_3$  on R-plane  $Al_2O_3$  after subtracting the background. Orange curve is the  $\Delta T/T$  dynamics of the bare R-plane  $Al_2O_3$  substrate measured in the same experimental conditions. The purple curve shows the intensity profile  $|E(t)|^2$  of the THz pump. Sample is at 300 K.

Such effect is clearly visible in the frequency domain where Fourier amplitude of the observed optical transmission oscillations show a narrow response where the pump spectrum has a negligible amplitude (Fig. 2a, b). The spectrum of the oscillatory component peaks at the  $A_{1g}$  phonon frequency measured by Raman spectroscopy, which matches the double of the frequency of the driving field (Fig. 2c). As one can see, the spectrum of the  $A_{1g}$  Raman spectrum shows a narrower line shape than the frequency response of the oscillations of the transmission modulation (Fig. 2b), because its spectral contents also depend on the frequency of the pump stimulus, which give rise to further broadening. This effect is also observed in  $V_2O_3$  with conventional pump-probe optical spectroscopy<sup>36</sup>. Furthermore, to exclude the contribution of other modes to the observed dynamics, we repeated the experiment on a  $V_2O_3$  thin film deposited on a C-plane (0001)  $Al_2O_3$  substrate, whose orientation results in a diagonal susceptibility tensor allowing only for the fully-symmetric  $A_{1g}$  modes to be detected (see Supplementary Note 3). The pump-probe dynamics of this sample also shows coherent oscillations peaked at the frequency of the  $A_{1g}$  phonon mode (see Supplementary Fig. 5), further demonstrating that the phonon generated by the THz excitation is the  $A_{1g}$  mode.

Figure 2d shows the dependence of the oscillation amplitude  $A$  on the electric field amplitude  $E^0$  of the incident THz field. The dependence is well described by a quadratic trend  $A = a(E^0)^2$  proving that the mode is nonlinearly coupled to the driving electric field. Moreover, as the spectral content of the pump pulse contains negligible intensity above 5 THz, we exclude a linear (dipolar) coupling of light to the lattice mode, which is in any case symmetry-forbidden since the mode is purely Raman active.

**THz displacive excitation of phonons.** Next, we discuss the nonlinear excitation mechanism of the vibrational modes by THz

driven electronic excitation. We propose that the interaction of the THz-frequency pulse with the metallic phase of  $V_2O_3$  first leads to the excitation of a time-dependent electronic distribution  $\eta(t)$  in the conduction bands. The time-domain dynamics of  $\eta(t)$  by THz excitation are described by:

$$\eta(t) = \kappa \int_0^\infty E^2(t - \tau)(e^{-\beta\tau} + c)d\tau, \quad (1)$$

where  $E(t)$  is the electric field temporal waveform of the THz pump pulse,  $1/\beta$  is the fast electronic relaxation rate after the THz excitation and  $c$  accounts for long-lived thermalization dynamics that last longer than 2 ps as also observed in  $V_2O_3$  by optical pump-probe spectroscopy<sup>36,39</sup>. The excited electronic states interact with the  $A_{1g}$  lattice mode *via* electron-phonon coupling and, in a semi-classical picture, they exert an effective force on the  $A_{1g}$  mode that has a time-dependence given by the intensity of the THz light field. According to general theory of DECP (see ref. 22), the effective force acting on the lattice associated with the electronic perturbation due to the intense time-varying electric field  $E(t)$  leads to the following equation of motion for the phonon displacement field:

$$\ddot{Q} + 2\gamma\dot{Q} + \Omega^2Q = \alpha\eta(t), \quad (2)$$

where  $Q$  is the normal coordinate of the  $A_{1g}$  phonon,  $\Omega/2\pi$  the phonon eigenfrequency,  $\gamma/2\pi$  the phonon damping rate<sup>36,39</sup> and  $\alpha$  the coupling constant. We model the THz-induced transmission modulation as the sum of the lattice and electronic contributions [Eqs. (1) and (2)], as described in ref. 22:

$$\Delta T/T(t_{pp}) = AQ(t_{pp}) + B\eta(t_{pp}), \quad (3)$$

with  $A$  and  $B$  multiplying constants.

Under this assumption, from Eq. (3) we calculated numerically the time-evolution of the transmission modulation dynamics

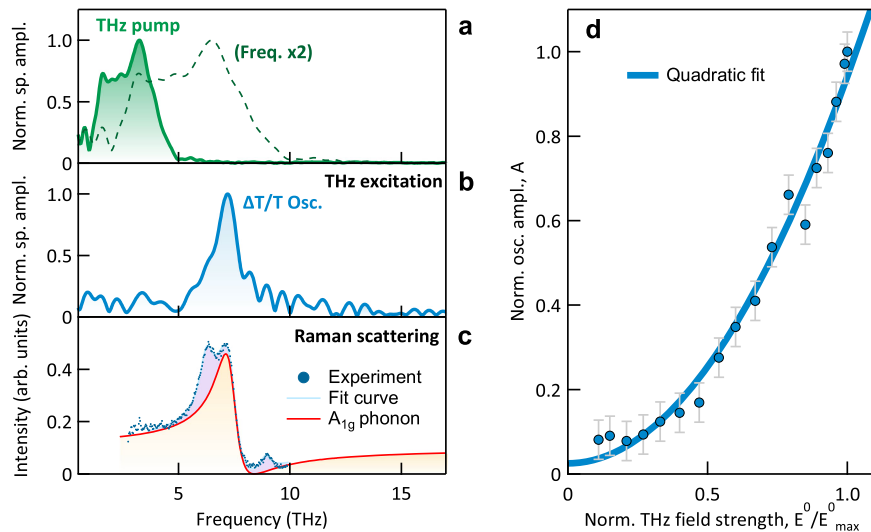


**Fig. 2 THz field-driven lattice phonon oscillations in frequency domain.** **a** Normalized spectral amplitude (Norm. sp. ampli.) of the THz pump pulse in Fig. 1d (green solid curve) and same spectrum with 2x frequency (green dashed curve). **b** Fourier transform of the oscillatory component of  $\Delta T/T$  for  $t_{pp} > 0.4$  ps (blue curve). **c** Raman spectroscopy of  $V_2O_3$  thin film at 300 K. Light blue dots are experimental data and light solid curve is the fit curve, which contains different spectral components: two  $E_g$  modes and the  $A_{1g}$ . The red curve is lineshape of the  $A_{1g}$  phonon, which is peaked at 7.1 THz. Vertical offset of -0.5 has been added to the experimental data for the overlap with the  $A_{1g}$  phonon lineshape. Data without offset is shown in Supplementary Fig. 4 and discussed in Supplementary Note 3. **d** Normalized oscillations amplitude (Norm. osc. ampli.) vs the normalized (Norm.) THz field strength,  $E_0/E_{peak}$ , with  $E_{peak} = 6.5$  MV/cm. The amplitude scales quadratically with the pump electric field (the light blue solid line represents a quadratic fit). Error bars indicate the standard deviations of the mean determined from pump-probe scan measurements with 15 acquisitions per point.

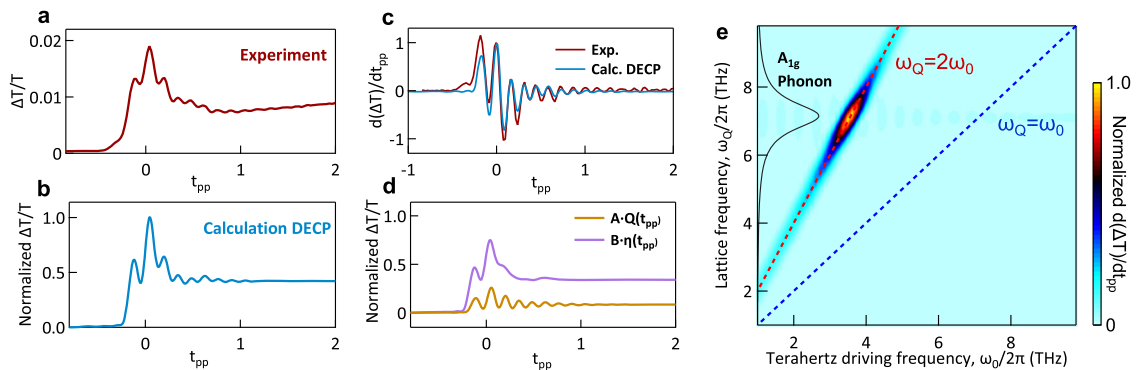


**Fig. 3 Modelling of terahertz displacive excitation of phonons.** **a** Experimental data at 300 K and **b**, numerical calculation using Eq. (3) using phononic and electronic parameters of  $V_2O_3$  at 300 K. **c** Comparison of the time derivative of the dynamics: experimental data (red curve) and numerical calculation (light blue curve), both normalized to the value at  $t_{pp} = 0$ . **d** Calculated electronic (blue curve) and lattice (red curve) contributions to the  $\Delta T/T$  dynamics from Eq. (3). The electron dynamics show no signature of long lived oscillatory components. **e** Time-derivative of the lattice dynamics  $Q(t)$  in frequency domain calculated by displacive excitation of coherent phonons (DECP) model [Eq. (2)] as a function of the center frequency  $\omega_0/2\pi$  of the driving THz field. Temporal derivative is shown to emphasize the oscillatory component over the slowly-varying background. The phonon amplitude is maximum when  $\Omega = 2\omega_0$ . The black curve is the  $A_{1g}$  phonon lineshape as a function of the lattice frequency  $\omega_Q/2\pi$ .

$\Delta T/T(t_{pp})$  by using the experimental THz driving field shown in Fig. 1c and the following  $A_{1g}$  phonon parameters  $\Omega/(2\pi) = 7.1$  THz,  $\gamma/(2\pi) = 0.5$  THz obtained by Raman spectroscopy (see Supplementary Note 3 and Supplementary Table 2). For the fast electronic relaxation dynamics after the THz excitation we set  $1/\beta = 80$  fs in agreement with ref. <sup>35</sup>. For the electron-phonon relaxation dynamics we set  $c = 0.2$  and  $B/A = 0.002$  to fit the amplitude of the experimental data. As expected from the numerical result of Eq. (3), the calculated dynamics by DECP model exhibits coherent lattice oscillations at twice the frequency of the electric field (Fig. 3a, b) and a step-like dynamics in agreement with the experiment, as also shown by the comparison of the corresponding time derivatives, see Fig. 3c. Figure 3d shows both the calculated electronic and lattice components of the dynamics from Eq. (3). As observed, the electronic dynamics has no long-lasting oscillating features.

Furthermore, we compute the lattice dynamics  $Q(t)$  by DECP model (Eq. (2)) as a function the driving frequency of THz pump. The numerical calculation of  $Q(t)$  is performed for multiple Gaussian THz pulses with a full width half maximum of 0.5 THz and center frequency  $\omega_0/2\pi$ , spanning from 1 to 10 THz with a frequency step of 0.125 THz. In Fig. 3e, we show the temporal derivative of  $Q(t)$  in frequency domain, which shows a maximum when THz driving frequency  $\omega_0/2\pi$  is half of the phonon frequency  $\omega_Q/2\pi$  as described by SFE, while no excitation is observed in resonant condition  $\omega_Q = \omega_0/2\pi$ .

**THz-induced dynamics across the temperature driven insulator-to-metal transition.** We now consider the temperature dependence of the oscillatory response. Figure 4a shows the phase

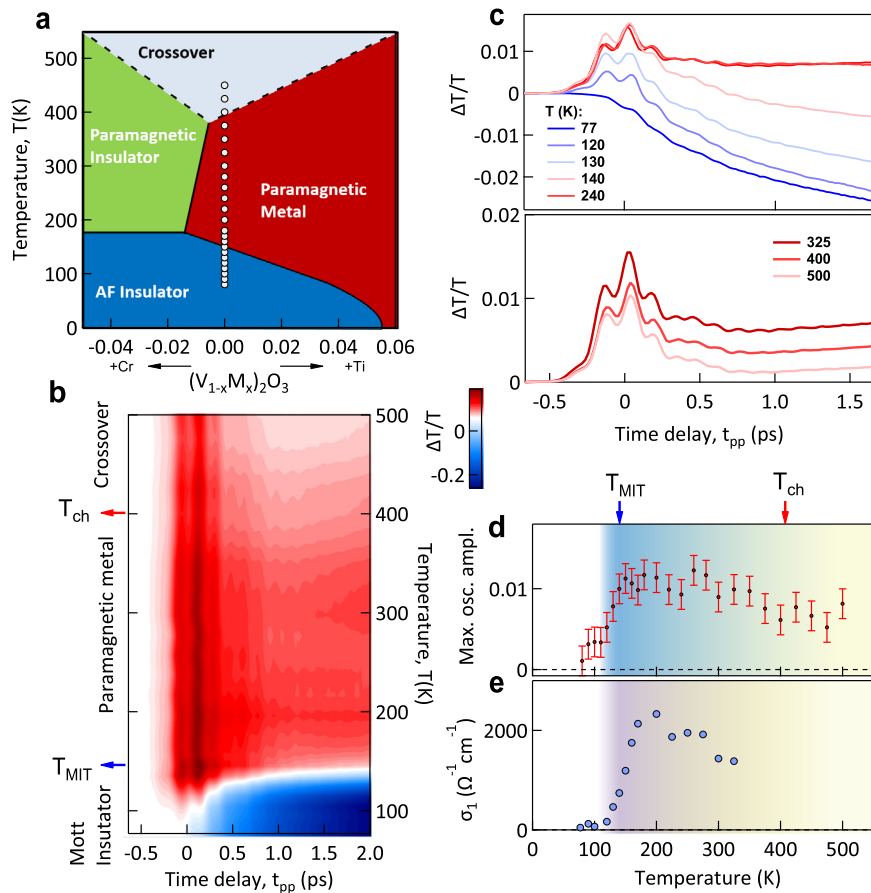


**Fig. 4 Temperature evolution of the sum-frequency excitation across the insulator to metal transition.** **a** Temperature vs doping phase diagram of  $V_2O_3$  according to ref. 44. The empty circles denote the values of the temperature measured in the present work. **b** Temperature dependence of the THz pump induced optical transmission modulation in  $V_2O_3$ . When the THz pulse interacts with the insulating Mott phase, no prominent signatures of lattice oscillation are observed.  $T_{MIT}$  indicates the metal-insulator transition temperature, while  $T_{ch}$  is the quasiparticle coherence temperature. **c** Pump-probe traces at selected temperatures. **d, e** Temperature dependence of the maximum oscillations amplitude (Max. osc. ampl.), **d**, and the real part of THz optical conductivity  $\sigma_1$  **e** of  $V_2O_3$ . THz optical conductivity of the  $V_2O_3$  film as a function of temperature was measured using Fourier-transform infrared spectroscopy in the THz range (see Supplementary Note 1). The color shading of **d, e** divides insulating phase and metallic phase. Error bars indicate the standard deviations of the mean determined from pump-probe scan measurements with 15 acquisitions per point.

diagram of  $(V_{1-x}M_x)_2O_3$ , where the dopant  $M$  is either Cr or Ti. We drive the temperature across the metal-to-insulator transition at  $x = 0$ . The temperature evolution of  $\Delta T/T(t_{pp})$  across the MIT is shown in Fig. 4b for various temperatures between 77 K and 500 K. In the insulating phase ( $T < T_{MIT}$ ) the transmission modulation displays a negative step-like component (see Fig. 4c) due to a partial formation of the metallic phase by the intense THz field<sup>41,42</sup>. However, the amplitude of coherent lattice vibrations is strongly reduced in the insulating phase (see Fig. 4d and Supplementary Fig. 7). In contrast, as the temperature approaches the MIT, we observe an emerging oscillatory signal at  $2\omega_p/2\pi$ , which denotes that the phonon excitation mechanism becomes efficient when the THz pump is resonant with the conduction states. By further increasing the temperature, the transmission modulation response rapidly decreases above the coherence temperature ( $T_{ch} \sim 400$  K), see Fig. 4d. This may be due to the suppression of the optical conductivity by means of the enhanced scattering rate of the electrons in the correlated electronic phase of  $V_2O_3$  at  $T_{MIT} < T < T_{ch}$ <sup>43,44</sup>. The amplitude of the oscillations versus the temperature strongly recalls the THz optical conductivity, as shown in the Fig. 4d, e. At present, an accurate model describing the transmission modulation response as a function of the temperature is still lacking, as it must account for the evolution of both the electronic phase and the lattice

structure across the different phases. We can, however, qualitatively understand the data shown in Fig. 4d, e by noting that the THz generated displacive force on the lattice coordinate (see Eq. (1) and ref. 22) is proportional to the deposited THz energy which is, in turn, proportional to the real part of the optical conductivity  $\sigma_1$  according to the Joule heating model:  $\int \sigma_1 E^2(t) dt$ , being the imaginary part  $\sigma_2$  of metallic phase negligible in the THz range<sup>45</sup>. Therefore the temperature trend of the phonon amplitude and of  $\sigma_1$  further supports the interpretation that the underlying generation mechanism is displacive rather than impulsive in nature.

## Discussion

We propose the following scenario to describe the mechanism for the nonlinear generation of a coherent  $A_{1g}$  phonon mode in  $V_2O_3$ . First, the incident THz field drives primarily intraband transitions in the  $a_{1g}$  electronic band of  $3d$  vanadium orbitals having the dominant contribution in the Drude spectral weight compared to the ones from the  $e_g^*$  band<sup>32</sup>. These newly populated states exert an effective force on the ions, driving a coherent  $A_{1g}$  symmetry mode. Okamoto et al.<sup>39</sup> have shown that Raman intensity of  $A_{1g}$  phonon modes are dominated by the electronic occupancy of  $a_{1g}$  band mediated by electron-phonon coupling<sup>39,46,47</sup>. Phenomenologically, the sum frequency excitation of the phonon mode in metallic  $V_2O_3$  can be

explained because the intense THz transient can temporally control the electronic distribution by intraband transitions in the  $a_{1g}$  bands, proportional to the THz intensity, leading to the coherent up-conversion excitation of the  $A_{1g}$  phonon mode. It is noteworthy that this process does not take place in insulating phase of  $V_2O_3$ , where the THz pulse is not coupled to  $a_{1g}$  electronic states, while non-resonant SFE is not observed because the Raman cross-section is lower than that of diamond crystal<sup>25</sup>. Finally, we note that time-resolved optical spectroscopy is not a priori able to determine the coefficients in Eq. (3); a quantitative disentangling of the electronic and lattice driven responses requires additional information that could be provided by future ultrafast x-ray or electron diffraction experiments to determine the magnitude of the coherent lattice displacements. An interesting connection exists between our observation of THz light-induced coherent phonon generation via stimulated Raman scattering from conductive electrons and the phenomenon of electrostriction in metals for DC electric fields. In electrostriction mechanism, an intense current in metals creates a strain field, proportional to the square of the electric field ( $E^2$ ), due to interaction of conduction electron states with acoustic phonon modes<sup>48</sup>. Electrostriction effects at THz frequencies have been reported in metallic films, where the strain waves driven by the intense THz field can generate mechanical fractures<sup>41,49</sup>.

Our observation of the coherent generation of Raman active phonons by THz excitation in a metallic system provides an interesting counterpart to ISRS- and DECP-based schemes in the infrared and visible ranges, using photons with much lower energy than the excited mode. This has the potential advantage of limiting the inevitable heating of the electronic system that necessarily occurs as a side effect of any scheme using light to coherently control the structure of metallic systems. This displacive excitation scheme may have potential advantages for applying coherent control methods to target other lattice-coupled collective modes, including magnons, for which sum-frequency ionic excitation has been recently discussed theoretically<sup>50</sup>, and provide new insights about the interplay between the lattice and other coexisting ordered phases.

## Methods

**Sample characterization and growth.** High-quality  $V_2O_3$  thin films were epitaxially grown on R-plane sapphire substrates by pulsed laser deposition using a KrF excimer laser beam focused with a fluence of  $1 \text{ J/cm}^2$  onto a ceramic  $V_2O_3$  bulk target. During the growth, the target was in an argon atmosphere of  $2 \cdot 10^{-2}$  mbar and the substrates were maintained at a temperature of 873 K, as described in ref. <sup>51</sup>. The high quality of the thin films was confirmed by diffraction analysis and electronic transport measurements as a function of temperature. The 84 nm-thin film of  $V_2O_3$  used in the experiment shows a resistivity change by more than four orders of magnitude between 40 K and 200 K. Raman spectroscopy of the  $V_2O_3$  film at 300 K (Fig. 3c) has been carried out using a LabRAM Series Raman Microscope (Horiba Jobin Yvon) equipped with a HeNe excitation laser ( $\lambda = 632.8 \text{ nm}$ ).

## Data availability

The data of the results presented in this paper, including those in the Supplementary Information, are available in Figshare with the identifier <https://doi.org/10.6084/m9.figshare.19312271.v1>.

Received: 11 October 2021; Accepted: 7 April 2022;

Published online: 28 April 2022

## References

- Juraschek, M. D. & Spaldin, N. A. Sounding out optical phonons. *Science* **357**, 873 (2017).
- Zhu, H. et al. Observation of chiral phonons. *Science* **359**, 579 (2018).
- Strohm, C., Rikken, G. L. J. A. & Wyder, P. Phenomenological evidence for the phonon Hall effect. *Phys. Rev. Lett.* **95**, 155901 (2005).
- Moya, X. & Mathur, N. D. Caloric materials near ferroic phase transitions. *Nat. Mater.* **13**, 439 (2014).
- Rini, M. et al. Control of the electronic phase of a manganite by mode-selective vibrational excitation. *Nature (Lond.)* **449**, 72 (2007).
- Fausti, D. et al. Light-induced superconductivity in a stripe-ordered cuprate. *Science* **331**, 189 (2011).
- Mitrano, M. et al. Possible light-induced superconductivity in  $K_3C_{60}$  at high temperature. *Nature (Lond.)* **530**, 461 (2016).
- Buzzi, M. et al. Photomolecular high-temperature superconductivity. *Phys. Rev. X* **10**, 031028 (2020).
- De la Torre, A. et al. Colloquium: Nonthermal pathways to ultrafast control in quantum materials. *Rev. Mod. Phys.* **93**, 041002 (2021).
- Nova, T. et al. An effective magnetic field from optically driven phonons. *Nat. Phys.* **13**, 132 (2017).
- Kubacka, T. et al. Large-amplitude spin dynamics driven by a THz pulse in resonance with an electromagnon. *Science* **343**, 1333 (2014).
- Maldovan, M. Sound and heat revolutions in phononics. *Nature (Lond.)* **503**, 209 (2013).
- Merlin, R. Generating coherent THz phonons with light pulses. *Solid State Commun.* **102**, 207 (1997).
- Huber, T., Ranke, M., Ferrer, A., Huber, L. & Johnson, S. L. Coherent phonon spectroscopy of non-fully symmetric modes using resonant terahertz excitation. *Appl. Phys. Lett.* **107**, 091107 (2015).
- Fu, Z. & Yamaguchi, M. Coherent excitation of optical phonons in GaAs by broadband terahertz pulses. *Sci. Rep.* **6**, 38264 (2016).
- Hase, M. et al. Optical control of coherent optical phonons in bismuth films. *Appl. Phys. Lett.* **69**, 2474 (1996).
- Kozina, M. et al. Terahertz-driven phonon upconversion in  $SrTiO_3$ . *Nat. Phys.* **15**, 387–392 (2019).
- Först, M. et al. Nonlinear phononics as an ultrafast route to lattice control. *Nat. Phys.* **7**, 854 (2011).
- Yan, Y. X. et al. Impulsive stimulated scattering: General importance in femtosecond laser pulse interactions with matter, and spectroscopic applications. *J. Chem. Phys.* **83**, 5391 (1985).
- Dahr, L. et al. Time-resolved vibrational spectroscopy in the impulsive limit. *Chem. Rev.* **94**, 157 (1994).
- Johnson, S. L. et al. Direct observation of non-fully-symmetric coherent optical phonons by femtosecond x-ray diffraction. *Phys. Rev. B* **87**, 054301 (2013).
- Zeiger, H. J. et al. Theory for displacive excitation of coherent phonons. *Phys. Rev. B* **45**, 768 (1992).
- Stevens, T. E., Kuhl, J. & Merlin, R. Coherent phonon generation and the two stimulated Raman tensors. *Phys. Rev. B* **65**, 144304 (2002).
- Shen, Y. R. & Bloembergen, N. Theory of stimulated Brillouin and Raman scattering. *Phys. Rev.* **137**, A1787 (1965).
- Maehrlein, S. F. et al. Terahertz sum-frequency excitation of a Raman-active phonon. *Phys. Rev. Lett.* **119**, 127402 (2017).
- Juraschek, D. M. & Maehrlein, S. F. Sum-frequency ionic Raman scattering. *Phys. Rev. B* **97**, 174302 (2018).
- Johnson, C. L., Knighton, B. E. & Johnson, J. A. Distinguishing nonlinear terahertz excitation pathways with two-dimensional spectroscopy. *Phys. Rev. Lett.* **122**, 073901 (2019).
- Knighton, B. E. et al. Terahertz waveform considerations for nonlinearly driving lattice vibrations. *J. Appl. Phys.* **125**, 144101 (2019).
- Melnikov, A. A., Selivanov, Y. G. & Chekalin, S. V. Phonon-driven ultrafast symmetry lowering in a  $Bi_2Se_3$  crystal. *Phys. Rev. B* **102**, 224301 (2020).
- Melnikov, A. A. et al. Coherent phonons in a  $Bi_2Se_3$  film generated by an intense single-cycle THz pulse. *Phys. Rev. B* **97**, 214304 (2018).
- Baldassarre, L. et al. Quasiparticle evolution and pseudogap formation in  $V_2O_3$ : An infrared spectroscopy study. *Phys. Rev. B* **77**, 113107 (2008).
- Qazilbash, M. M. et al. Electrodynamics of the vanadium oxides  $VO_2$  and  $V_2O_3$ . *Phys. Rev. B* **77**, 115121 (2008).
- Liu, M. K. et al. Photoinduced phase transitions by time-resolved far-infrared spectroscopy in  $V_2O_3$ . *Phys. Rev. Lett.* **107**, 066403 (2011).
- Abreu, E. et al. Ultrafast electron-lattice coupling dynamics in  $VO_2$  and  $V_2O_3$  thin films. *Phys. Rev. B* **96**, 094309 (2017).
- Lantz, G. et al. Ultrafast evolution and transient phases of a prototype out-of-equilibrium Mott-Hubbard material. *Nat. Commun.* **8**, 13917 (2017).
- Misochko, O. V. et al. Phonons in  $V_2O_3$  above and below the Mott transition: A comparison of time- and frequency-domain spectroscopy results. *Phys. B: Condens. Matter* **263**, 57 (1999).
- Mansart, B. et al. Mott transition in Cr-doped  $V_2O_3$  studied by ultrafast reflectivity: Electron correlation effects on the transient response. *Europhys. Lett.* **92**, 37007 (2010).
- Gerber, S. et al. Femtosecond electron-phonon lock-in by photoemission and x-ray free-electron laser. *Science* **357**, 71 (2017).

39. Okamoto, A. et al. Raman Study on the High Temperature Transition in  $V_2O_3$ . *J. Phys. Soc. Jpn.* **52**, 312 (1983).
40. von Hoegen, A. et al. Probing the interatomic potential of solids with strong-field nonlinear phononics. *Nature* **555**, 79 (2018).
41. Giorgianni, F., Sakai, J. & Lupi, S. Overcoming the thermal regime for the electric-field driven Mott transition in vanadium sesquioxide. *Nat. Commun.* **10**, 1159 (2019).
42. Gray, A. X. et al. Ultrafast terahertz field control of electronic and structural interactions in vanadium dioxide. *Phys. Rev. B* **98**, 045104 (2018).
43. Lo Vecchio, I. et al. Orbital dependent coherence temperature and optical anisotropy of  $V_2O_3$  quasiparticles. *J. Phys.: Condens. Matter* **29**, 345602 (2017).
44. Lo Vecchio, I. et al. Optical properties of  $V_2O_3$  in its whole phase diagram. *Phys. Rev. B* **91**, 155133 (2015).
45. Luo, Y. Y. et al. Terahertz transport dynamics in the metal-insulator transition of  $V_2O_3$  thin film. *Opt. Commun.* **387**, 385 (2017).
46. Tian, Y. T. et al. Ultrafast dynamics Evidence of High Temperature Superconductivity in Single Unit Cell FeSe on SrTiO<sub>3</sub>. *Phys. Rev. Lett.* **116**, 107001 (2016).
47. Wu, Q. et al. Ultrafast Quasiparticle Dynamics and Electron-Phonon Coupling in  $(Li_{0.84}Fe_{0.16})OHFe_{0.98}Se$ . *Chin. Phys. Lett.* **37**, 097802 (2020).
48. Kornreich, P., Callen, H. & Gundjian, A. Current Striction-A Mechanism of Electrostriction in Many-Valley Semiconductors. *Phys. Rev.* **161**, 815 (1967).
49. Agranet, M. B. et al. Damage in a thin metal film by high-power terahertz radiation. *Phys. Rev. Lett.* **120**, 085704 (2018).
50. Juraschek, D., Wang, D. S. & Narang, P. Sum-frequency excitation of coherent magnons. *Phys. Rev. B* **103**, 094407 (2021).
51. Sakai, J., Limelette, P. & Funakubo, H. Transport properties and  $c/a$  ratio of  $V_2O_3$  thin films grown on C- and R-plane sapphire substrates by pulsed laser deposition. *Appl. Phys. Lett.* **107**, 241901 (2015).

## Acknowledgements

We thank Lara Benfatto for the fruitful discussion and for critical reading of the manuscript. We are grateful to Hans-Heinrich Braun, Carlo Vicario and the PSI-LNO group for support. We acknowledge financial support by Swiss National Science Foundation project no. IZLRZ2\_164051, by MAECI under the Italian-India collaborative project SUPERTOP-PGR04879 and by EC FP7 Graphene Flagship Project No. CNECTICT-604391. The research was supported by the NCCR MUST, founded by the Swiss National Science Foundation, and by ERC Grant Hyper Quantum Criticality (HyperQC). MR and MC acknowledges the support of SNF Project No. 200021\_182695.

## Author contributions

F.G. conceived and designed the experiment with S.L.J.'s supervision. E.P., M.C., M.R., and J.S. grew the samples and performed structural characterizations and transport measurements. F.G. carried out the THz experiments with the support of the PSI-NLO staff. F.G. prepared the figures for the manuscript. C.W.S. and F.G. performed the Raman spectroscopy measurements. M.U., F.G., and T.C. interpreted the data through DECP theory and performed calculations. L.B. and F.G. performed THz spectroscopy measurements. F.G. and S.L.J. wrote the manuscript. All authors extensively discussed the results.

## Competing interests

The authors declare no competing interests.

## Additional information

**Supplementary information** The online version contains supplementary material available at <https://doi.org/10.1038/s42005-022-00882-7>.

**Correspondence** and requests for materials should be addressed to Flavio Giorgianni.

**Peer review information** *Communications Physics* thanks the anonymous reviewers for their contribution to the peer review of this work. Peer reviewer reports are available.

**Reprints and permission information** is available at <http://www.nature.com/reprints>

**Publisher's note** Springer Nature remains neutral with regard to jurisdictional claims in published maps and institutional affiliations.



**Open Access** This article is licensed under a Creative Commons Attribution 4.0 International License, which permits use, sharing, adaptation, distribution and reproduction in any medium or format, as long as you give appropriate credit to the original author(s) and the source, provide a link to the Creative Commons license, and indicate if changes were made. The images or other third party material in this article are included in the article's Creative Commons license, unless indicated otherwise in a credit line to the material. If material is not included in the article's Creative Commons license and your intended use is not permitted by statutory regulation or exceeds the permitted use, you will need to obtain permission directly from the copyright holder. To view a copy of this license, visit <http://creativecommons.org/licenses/by/4.0/>.

© The Author(s) 2022